MICROBOONE-NOTE-1132-PUB

Search for a Sterile Neutrino in a 3+1 Framework using Wire-Cell Inclusive Charged-Current ν_e Selection with the BNB and NuMI beamlines in MicroBooNE

The MicroBooNE collaboration
microboone_info@fnal.gov

June 7, 2024

Contents

1 INTRODUCTION

While most neutrino oscillation measurements are consistent with the three-neutrino framework (see Ref. [1, 2] among others), the existence of a light eV-scale sterile neutrino has been postulated to explain several experimental anomalies: (1) the observation that calibrated ν_e sources (^{51}Cr for GALLEX [3] and BEST [4], ^{51}Cr and ^{37}Ar for SAGE [5]) observed lower rates of ν_e interactions than expected in the three-neutrino framework, which could be explained by ν_e disappearance considering light sterile neutrinos; (2) the reactor anti-neutrino anomaly [6], where the observed deficit in the measured $\bar{\nu}_e$ events relative to the expectation based on the recent reactor anti-neutrino flux calculations [7, 8] could be explained by $\bar{\nu}_e$ disappearance considering light sterile neutrinos, although there are recent experimental measurements [9, 10] and improved flux calculations [11, 12] that disfavor this explanation; (3) the Neutrino-4 [13] anomaly, which suggests reactor $\bar{\nu}_e$ oscillation at a few meters; and (4) the anomalous excess of electron-neutrino-like events in LSND [14] and the excess of low-energy electron-like (LEE) events in MiniBooNE [15, 16], which suggest ν_e appearance from ν_μ to ν_e oscillations as might occur considering light sterile neutrinos. However, there are significant challenges in explaining all available experimental results with a sterile neutrino oscillation model in a global fit [17]. Nevertheless, it is important to clarify these experimental anomalies. Moreover, a sterile neutrino, if discovered, would have a profound impact on not only particle physics but also astrophysics and cosmology such as in large-scale structure formation [18] and leptogenesis [19].

The recent distinct and complementary low-energy excess searches at MicroBooNE [20, 21, 22, 23], which aim to provide a definite check on the MiniBooNE LEE, show that "the results are found to be consistent with the nominal ν_e rate expectations from the Booster Neutrino Beam (BNB) [24] and no excess of ν_e events is observed", assuming a simple LEE template unfolded from the MiniBooNE excess. While these results suggest the MiniBooNE LEE has a non-ν_e origin, the current results may still be compatible with the hypothesis of a light sterile neutrino suggested by remaining experimental anomalies (GALLEX [3], BEST [4], SAGE [5], Neutrino-4 [13], and LSND [14]).

In order to fully evaluate the possible existence of sterile neutrinos using the MicroBooNE data, a 3+1 (three flavors of standard model neutrinos + one flavor of sterile neutrino) neutrino oscillation analysis was carried out previously, using only BNB data [25]. The high-performance neutrino selection and well-understood systematic uncertainties of the ν_e and ν_μ event rate predictions in the recent MicroBooNE LEE analysis using Wire-Cell reconstruction [23] was used, and the 3+1 oscillation analysis results for several different scenarios considering the oscillation effects from (1) ν_e appearance only (ν_μ to ν_e oscillation), (2) ν_e disappearance only, and (3) ν_e appearance + ν_e and ν_μ disappearance was presented. The sensitivity of our first result is impacted by a potential cancellation of ν_e appearance and disappearance. This degeneracy in the oscillation signature is primarily impacted by the relative content of ν_μ and ν_e in the beam. The addition of data from the Neutrinos at the Main Injector (NuMI) beamline (a second neutrino beam where off-axis neutrinos incidentally illuminate the MicroBooNE detector) in a joint oscillation measurement can mitigate this degeneracy enhancing the analysis' sensitivity thanks to the different overall ν_μ -to-ν_e ratio of the two beams.

In this note, we show the sensitivity improvement by adding in data collected from the NuMI beam during 2015-18 in the same analysis framework. In addition, a validation of the NuMI flux prediction at MicroBooNE [26] is performed.

2 Analysis approach

In this analysis, we consider the 3+1 neutrino framework, which is the simplest extension of the standard 3ν framework with the addition of a non-standard massive (sterile) neutrino at the eV scale. The flavor and mass eigenstates are connected by a 4×4 mixing matrix

$$\begin{pmatrix} \nu_e \\ \nu_\mu \\ \nu_\tau \\ \nu_s \end{pmatrix} = \begin{pmatrix} U_{e1} & U_{e2} & U_{e3} & U_{e4} \\ U_{\mu 1} & U_{\mu 2} & U_{\mu 3} & U_{\mu 4} \\ U_{\tau 1} & U_{\tau 2} & U_{\tau 3} & U_{\tau 4} \\ U_{s1} & U_{s2} & U_{s3} & U_{s4} \end{pmatrix} \begin{pmatrix} \nu_1 \\ \nu_2 \\ \nu_3 \\ \nu_4 \end{pmatrix}. \tag{1}$$

The oscillation probability from α-flavor to β-flavor type neutrino in vacuum can be expressed as

$$P_{\nu_\alpha \to \nu_\beta} = \delta_{\alpha\beta} - 4\sum_{i>j} Re(U_{\beta i} U^*_{\alpha i} U_{\beta j} U^*_{\alpha j}) \sin^2\Delta_{ij} + 2\sum_{i>j} Im(U_{\beta i} U^*_{\alpha i} U_{\beta j} U^*_{\alpha j}) \sin 2\Delta_{ij}, \tag{2}$$

where $\alpha, \beta = e, \mu, \tau, s$, and $i, j = 1, 2, 3, 4$. Δ_{ij} stands for

$$\Delta_{ij} \equiv \frac{\Delta m^2_{ij} L}{4E} = 1.267 \left(\frac{\Delta m^2_{ij}}{\mathrm{eV}^2}\right) \left(\frac{\mathrm{MeV}}{E}\right) \left(\frac{L}{m}\right) \tag{3}$$

where $\Delta m^2_{ij} = m^2_i - m^2_j$ is the mass-squared difference between the neutrino mass eigenstates ν_i and ν_j.

Since m_4 is at eV-scale ($m_4 \gg m3, m2, m1$) and the MicroBooNE experiment has a short baseline, there is effectively only one mass-squared difference Δm^2_{41} appearing in the oscillation formula. The three main oscillation channels: $\nu_e \to \nu_e$, $\nu_\mu \to \nu_\mu$, and $\nu_\mu \to \nu_e$, have the following oscillation probabilities:

$$P_{\nu_e \to \nu_e} = 1 - 4(1 - |U_{e4}|^2)|U_{e4}|^2 \sin^2\Delta_{41}, \tag{4}$$

$$P_{\nu_\mu \to \nu_\mu} = 1 - 4(1 - |U_{\mu 4}|^2)|U_{\mu 4}|^2 \sin^2\Delta_{41}, \tag{5}$$

$$P_{\nu_\mu \to \nu_e} = 4|U_{\mu 4}|^2 |U_{e4}|^2 \sin^2\Delta_{41}. \tag{6}$$

The matrix element terms are often replaced with effective mixing angles

$$\sin^2 2\theta_{ee} = 4(1-|U_{e4}|^2)|U_{e4}|^2, \tag{7}$$
$$\sin^2 2\theta_{\mu\mu} = 4(1-|U_{\mu 4}|^2)|U_{\mu 4}|^2, \tag{8}$$
$$\sin^2 2\theta_{\mu e} = 4|U_{\mu 4}|^2|U_{e4}|^2. \tag{9}$$

The $\nu_e \to \nu_s$ and $\nu_\mu \to \nu_s$ oscillation probabilities, which are important for the neutral-current interaction channel, are

$$P_{\nu_e\to\nu_s} = 4|U_{e4}|^2|U_{s4}|^2\sin^2\Delta_{41}, \tag{10}$$
$$P_{\nu_\mu\to\nu_s} = 4|U_{\mu 4}|^2|U_{s4}|^2\sin^2\Delta_{41}. \tag{11}$$

Similarly, we can replace the matrix terms with effective mixing angles

$$\sin^2 2\theta_{es} = 4|U_{e4}|^2|U_{s4}|^2, \tag{12}$$
$$\sin^2 2\theta_{\mu s} = 4|U_{\mu 4}|^2|U_{s4}|^2. \tag{13}$$

Here, the 4×4 mixing matrix can be parameterized as below ensuring the unitarity of the mixing matrix [27],

$$U = R_{34}(\theta_{34},\delta_{34})R_{24}(\theta_{24},\delta_{24})R_{14}(\theta_{14},0)R_{23}(\theta_{23},0)R_{13}(\theta_{13},\delta_{13})R_{12}(\theta_{12},0) \tag{14}$$

where $R_{ij}(\theta_{ij},\delta_{ij})$ denotes a counterclockwise rotation in the complex ij-plane through a mixing angle θ_{ij} and a CP phase δ_{ij}. Table 1 shows the connections between the mixing angles and the mixing matrix terms.

Table 1: 3+1 sterile neutrino mixing parameters and the effective angles.

$\sin^2 2\theta_{ee}$	$= \sin^2 2\theta_{14}$	$= 4(1-\lvert U_{e4}\rvert^2)\lvert U_{e4}\rvert^2$
$\sin^2 2\theta_{\mu\mu}$	$= 4\cos^2\theta_{14}\sin^2\theta_{24}\left(1-\cos^2\theta_{14}\sin^2\theta_{24}\right)$	$= 4(1-\lvert U_{\mu 4}\rvert^2)\lvert U_{\mu 4}\rvert^2$
$\sin^2 2\theta_{\mu e}$	$= \sin^2 2\theta_{14}\sin^2\theta_{24}$	$= 4\lvert U_{\mu 4}\rvert^2\lvert U_{e4}\rvert^2$
$\sin^2 2\theta_{es}$	$= \sin^2 2\theta_{14}\cos^2\theta_{24}\cos^2\theta_{34}$	$= 4\lvert U_{e4}\rvert^2\lvert U_{s4}\rvert^2$
$\sin^2 2\theta_{\mu s}$	$= \cos^4\theta_{14}\sin^2 2\theta_{24}\cos^2\theta_{34}$	$= 4\lvert U_{\mu 4}\rvert^2\lvert U_{s4}\rvert^2$

It should be noted that the ν_e disappearance oscillation effect can cancel the ν_e oscillation effect in the observed ν_e CC events, resulting in a degeneracy in the estimated oscillation parameters. This cancellation is expressed in in the equation

$$N_{\nu_e} = N_{\text{intrinsic }\nu_e} \cdot P_{\nu_e \to \nu_e} + N_{\text{intrinsic }\nu_\mu} \cdot P_{\nu_\mu \to \nu_e} \tag{15}$$

$$= N_{\text{intrinsic }\nu_e} \cdot \left[1 + (R_{\nu_\mu/\nu_e} \cdot \sin^2\theta_{24} - 1) \cdot \sin^2 2\theta_{14} \cdot \sin^2\Delta_{41} \right], \tag{16}$$

where R_{ν_μ/ν_e} is the ratio of intrinsic ν_μ and ν_e events in the beam as a function of true neutrino energy. In the case of the BNB, the degeneracy of $\sin^2\theta_{24}$ and $\sin^2 2\theta_{14}$ happens when $\sin^2\theta_{24} \approx 0.005$ given $R_{\nu_\mu/\nu_e} \approx 185$. This degeneracy is mitigated by adding data from NuMI beamline, where $R_{\nu_\mu/\nu_e} \approx 21$. Figure 1 shows that the intrinsic flux and ν_μ to ν_e ratio in NuMI is quite different from that in BNB across the relevant range of energies.

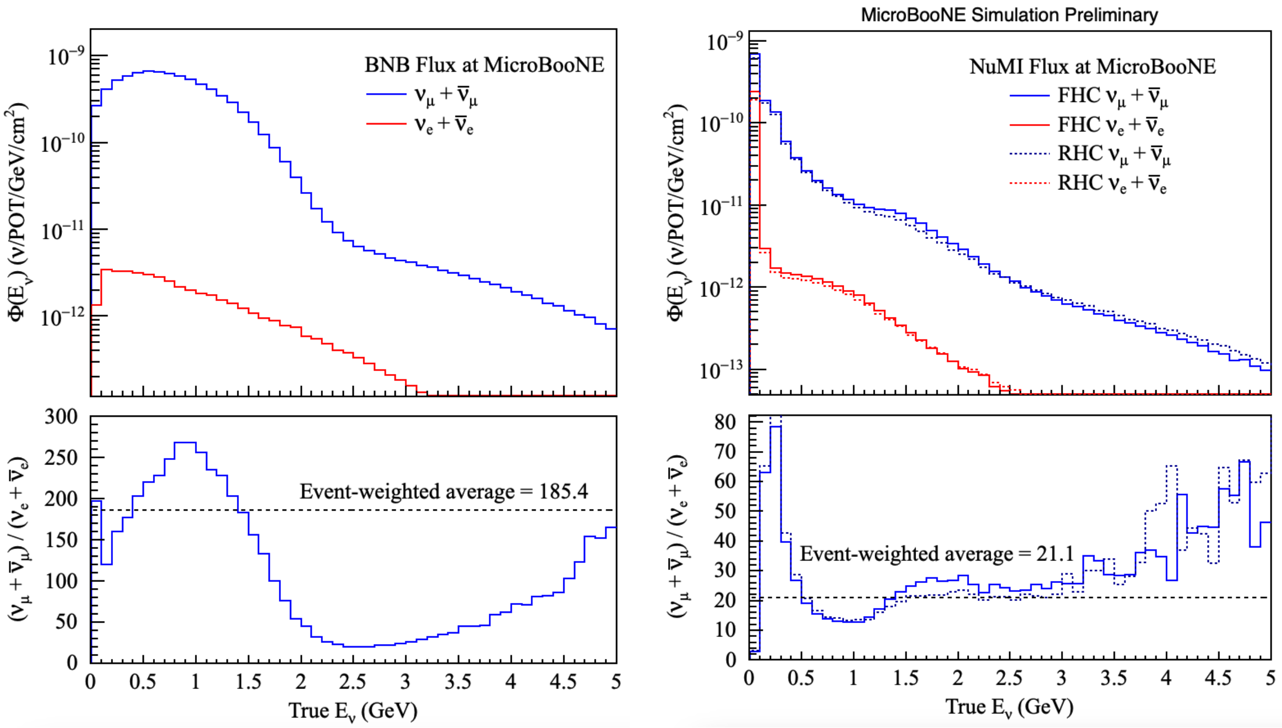

(a) BNB flux **(b)** NuMI flux

Figure 1: BNB (a) and NuMI (b) instrinsic ν_e and ν_μ flux and their ratios as a function of true neutrino energy. For NuMI, FHC (forward horn current, solid lines) and RHC (reverse horn current, dashed lines) predictions are shown together.

Figure 2 illustrates the predicted energy spectra of the BNB and NuMI ν_e CC FC channels at different values of the oscillation parameters[1]: (a) no oscillation effect (black solid line), (b) both disappearance and appearance oscillation effects with ($\Delta m^2_{14} = 7.3$ eV^2, $\sin^2 2\theta_{14} = 0.36$, $\sin^2\theta_{24} = 0.01$) (blue solid line), (c) both disappearance and appearance oscillation effects with ($\Delta m^2_{14} = 7.3$ eV^2, $\sin^2 2\theta_{14} = 0.36$, $\sin^2\theta_{24} = 0.005$) (red solid line), and (d) both disappearance and appearance oscillation effects with ($\Delta m^2_{14} = 7.3$ eV^2, $\sin^2 2\theta_{14} = 0.72$, $\sin^2\theta_{24} = 0.005$) (red dashed line).

In BNB, the scenario (b) show obvious oscillation effects. The scenarios (c) and (d) show weak

[1]Note that ν_e CC channels contain both ν_e and $\bar{\nu}_e$ components. The $\bar{\nu}_e$ rate is negligible in BNB ν_e CC selection, whereas in the NuMI ν_e CC selection, it constitutes 1/5 of the ν_e .

oscillation effect below 1500 MeV, which is because of the cancellation between ν_e disappearance and appearance, especially when $\sin^2\theta_{24}$ approaches 0.005. This shows the impact of the degeneracy in the BNB ν_e dataset.

In NuMI, this degeneracy is broken due to the different R_{ν_μ/ν_e}, so there's no such degeneracy with $\sin^2\theta_{24} = 0.005$. One can see that the scenario (c) and (d) result in very different spectra, causing no degeneracy in $\sin^2 2\theta_{14}$ for NuMI. Also, in both cases, the impact of oscillations on the energy spectrum is clearly visible.

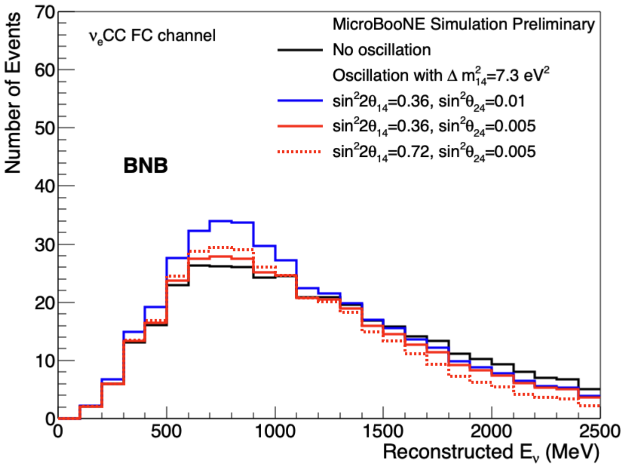

(a) BNB reconstructed neutrino energy spectrum

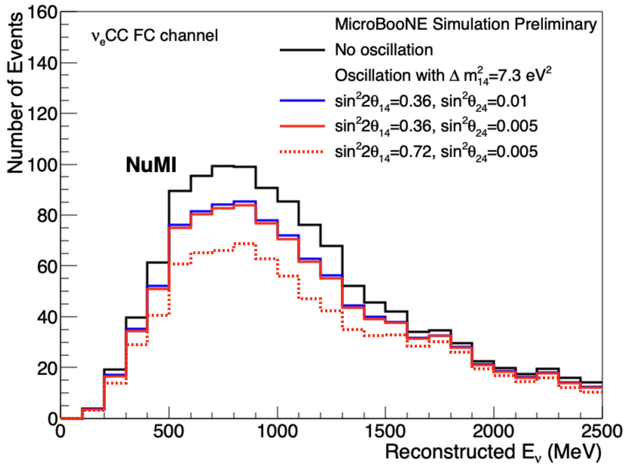

(b) NuMI reconstructed neutrino energy

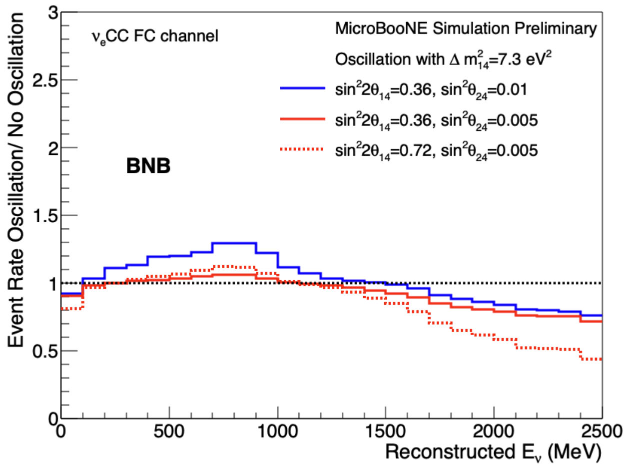

(c) BNB event rate ratio

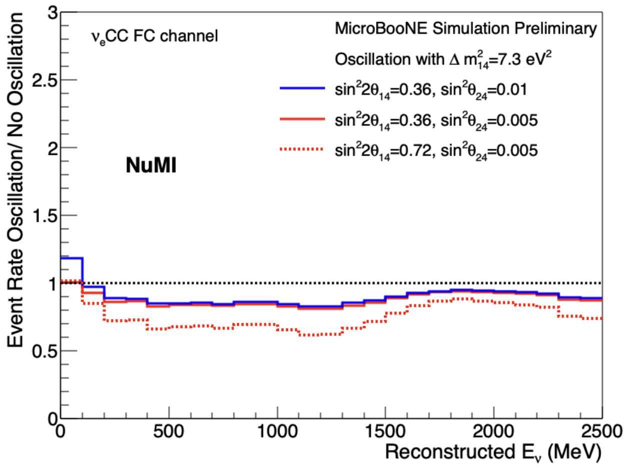

(d) NuMI event rate ratio

Figure 2: Energy spectra and event rate ratio of oscillation/no oscillation for the BNB and NuMI ν_e CC FC channel at different values of the oscillation parameters.

Figure 3 shows a similar study, but with different oscillation parameters. Here we pick $\Delta m^2_{14} = 1.2$ eV^2, $\sin^2 2\theta_{\mu e} = 0.003$, and compared different predicted energy spectrum of the BNB and NuMI ν_e CC FC channels: (a) no oscillation effect (black solid line), (b) both disappearance and appearance oscillation effects with ($\Delta m^2_{14} = 1.2$ eV^2, $\sin^2 2\theta_{\mu e} = 0.003$, $\sin^2\theta_{24} = 0.018$) (red dashed line), and (c) both disappearance and appearance oscillation effects with ($\Delta m^2_{14} = 1.2$ eV^2, $\sin^2 2\theta_{\mu e} = 0.003$, $\sin^2\theta_{24} = 0.0045$) (greed solid line). Here, $\sin^2\theta_{24}$ values were chosen based on preferred value with either the combined BNB and NuMI Asimov dataset, or the BNB-only data.

Similar to the study in Fig. 2, case (b) shows clear oscillation effect in BNB, where case (c) with weak oscillation effect with $\sin^2\theta_{24}$ close to the degeneracy point $\sin^2\theta_{24} = 0.005$. In NuMI, this degeneracy is broken as case (c) shows the strong oscillation with no degeneracy in this oscillation parameter values.

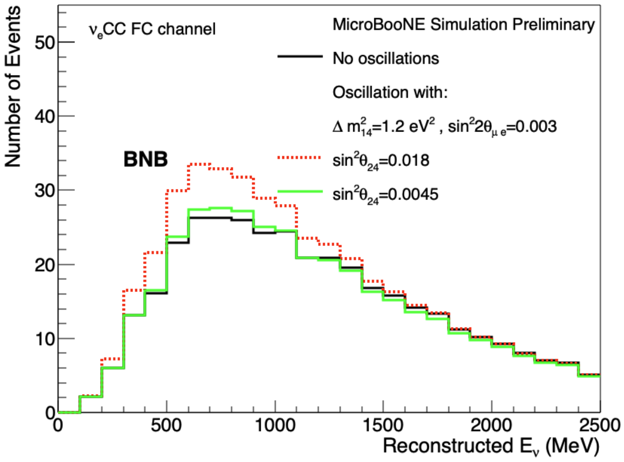

(a) BNB reconstructed neutrino energy spectrum

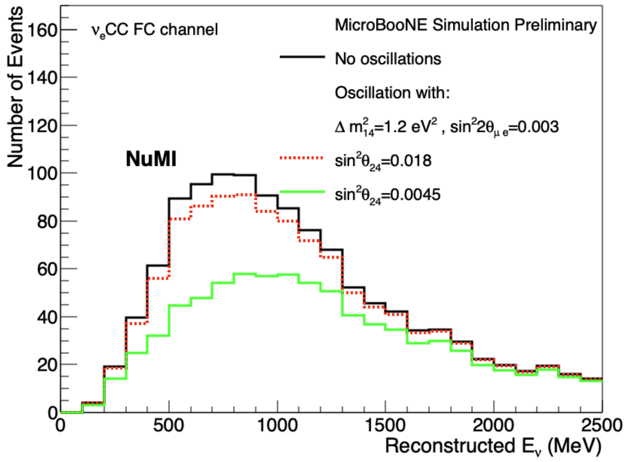

(b) NuMI reconstructed neutrino energy

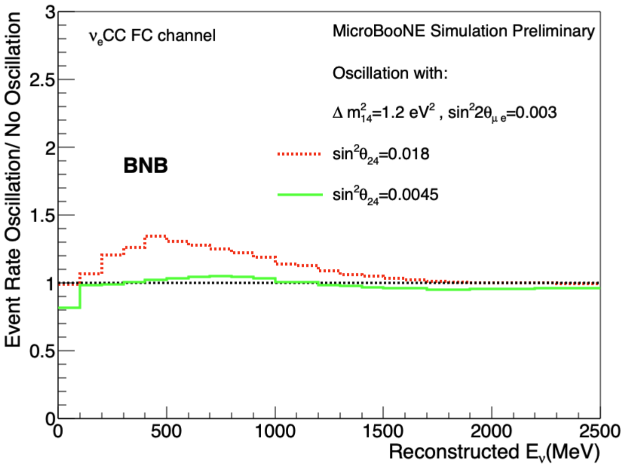

(c) BNB event rate ratio

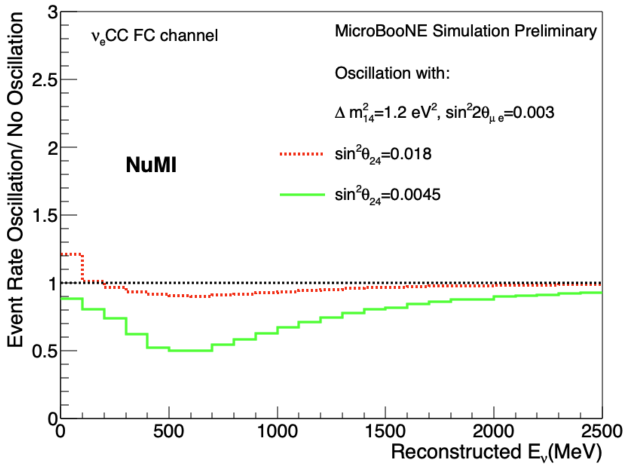

(d) NuMI event rate ratio

Figure 3: Energy spectra and event rate ratio of oscillation/no oscillation for the BNB and NuMI ν_e CC FC channel at different values of the oscillation parameters.

3 Analysis Status

3.1 ν_μ CC data/MC with updated NuMI flux

As described in Ref. [26], the NuMI flux prediction at MicroBooNE was recently modified to include several updates:

- Shielding block geometry update
- Geant4 version update from v4.9.2 to v4.10.4
- Updated PPFX implementation accounting for the underlying changes in the simulation

The MicroBooNE collaboration has developed a reweighting scheme in order to reflect these changes in the NuMI flux prediction, with more details in Ref. [26]. With this new NuMI flux prediction, the overall uncertainty on the NuMI flux is about 20%. We have checked the validity of the new flux prediction and its uncertainty by looking at the sideband samples, ν_μ CC fully-contained (FC) and partially-contained (PC) events.

Figure 4 shows the reconstructed neutrino energy spectrum of NuMI Run1-3 ν_μ CC FC and PC samples. We observe an underprediction of Monte-Carlo (MC), especially at lower energies, with about 26% lower than data. However, the offset is consistent at the 1 σ level within the systematics.

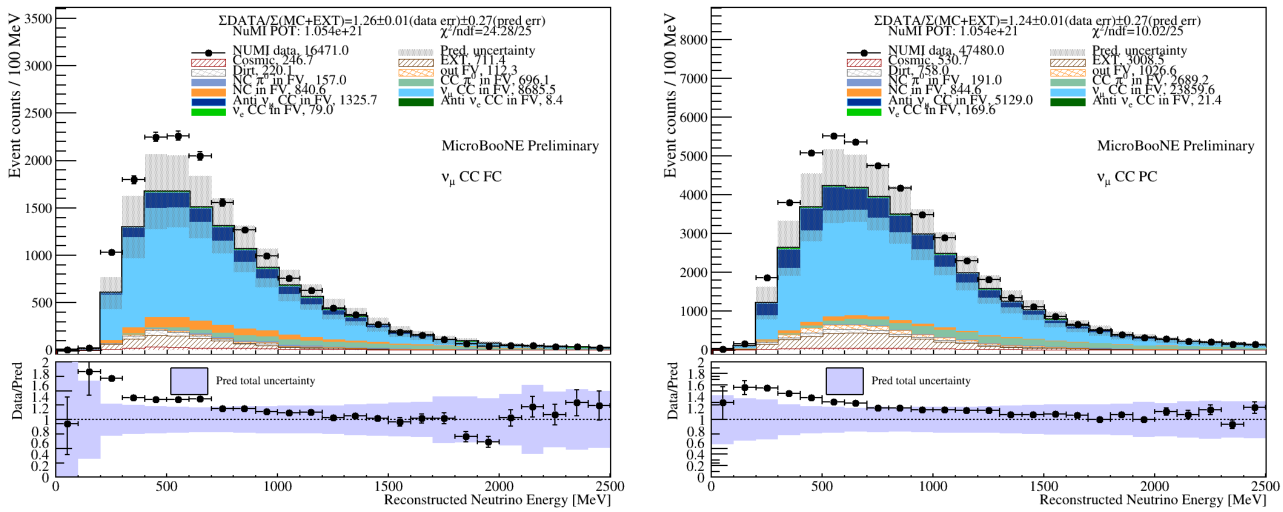

(a) NuMI ν_μ CC FC

(b) NuMI ν_μ CC PC

Figure 4: Reconstructed neutrino energy spectrum of NuMI Run1-3 ν_μ CC FC (a) and PC (b) sample using data and updated MC samples. The breakdown of each component for different final states for both signal and background events is shown in the legend. The bottom sub-panel presents the data-to-prediction ratios as well as the full systematic uncertainty of MC prediction.

In order to further validate the newly updated NuMI flux prediction and its uncertainty, we have performed a conditional constraint study using the BNB ν_μ CC FC sample. The conditional covariance matrix formalism [28] was used for the study, where we derive the conditional mean and conditional variance of the prediction of target channel (NuMI ν_μ CC FC in Fig. 6a or NuMI ν_μ CC PC sample in Fig. 6b), given the constraints from the measurement of constraining channels (BNB

ν_μ CC FC in Fig. 6a or NuMI ν_μ CC FC sample in Fig. 6b). This allows more information about the compatibility between the model and data.

Figure 5 shows the energy spectrum of both the BNB and NuMI ν_μ CC FC samples with the total unconstrained systematic uncertainty, and Fig. 6 shows the NuMI ν_μ CC FC constrained by the BNB ν_μ CC FC sample and the NuMI ν_μ CC PC sample constrained by the NuMI ν_μ CC FC sample. When constraining the NuMI ν_μ CC FC prediction using the BNB ν_μ CC FC observed data, the correlated cross-section and detector systematic uncertainties are strongly suppressed. The flux systematics are unchanged by the constraint since they are treated as uncorrelated. Hence, the remaining uncertainty is dominated by the flux uncertainty. The data and constrained prediction show good agreement, within flux-dominated systematics, demonstrating that the updated flux prediction agrees well with the data well within the uncertainty. This can further be checked by constraining the NuMI ν_μ CC PC by NuMI ν_μ CC FC sample, where the conditional constraints suppress all the systematic errors leading to a significantly reduced uncertainty. The data and constrained prediction agrees very well within the remaining uncertainty with $\chi^2/ndf = 13.76/25$.

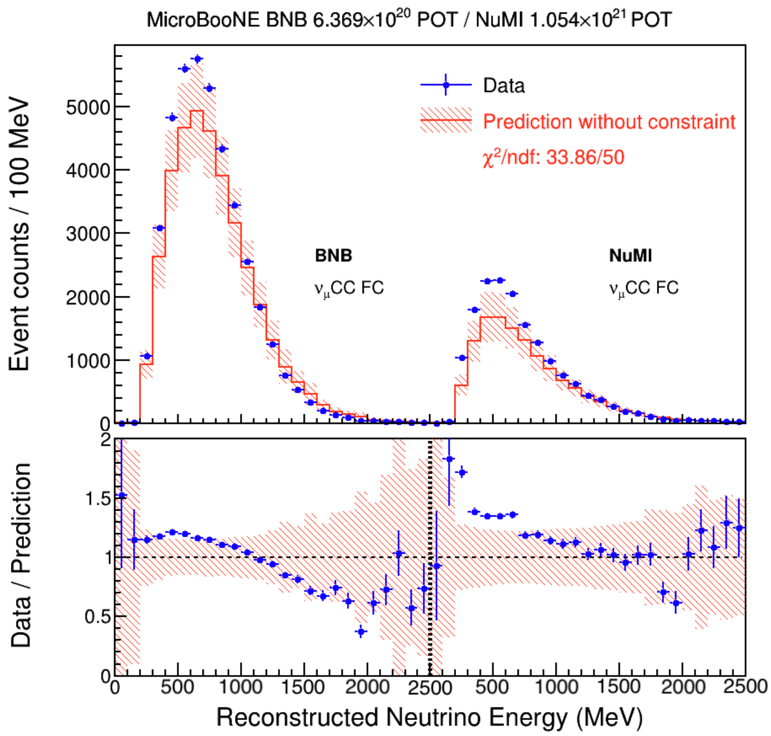

Figure 5: Reconstructed energy spectrum of BNB Run1-3 and NuMI Run1-3 ν_μ CC FC sample. The red band represents the total systematic uncertainty. The bottom sub-panel presents the data-to-prediction ratio as well as the full systematic uncertainty of MC prediction.

In summary, we have observed that our updated NuMI flux prediction agrees well with ν_μ data observations within systematic uncertainties, validating the usage of this flux for this oscillation analysis.

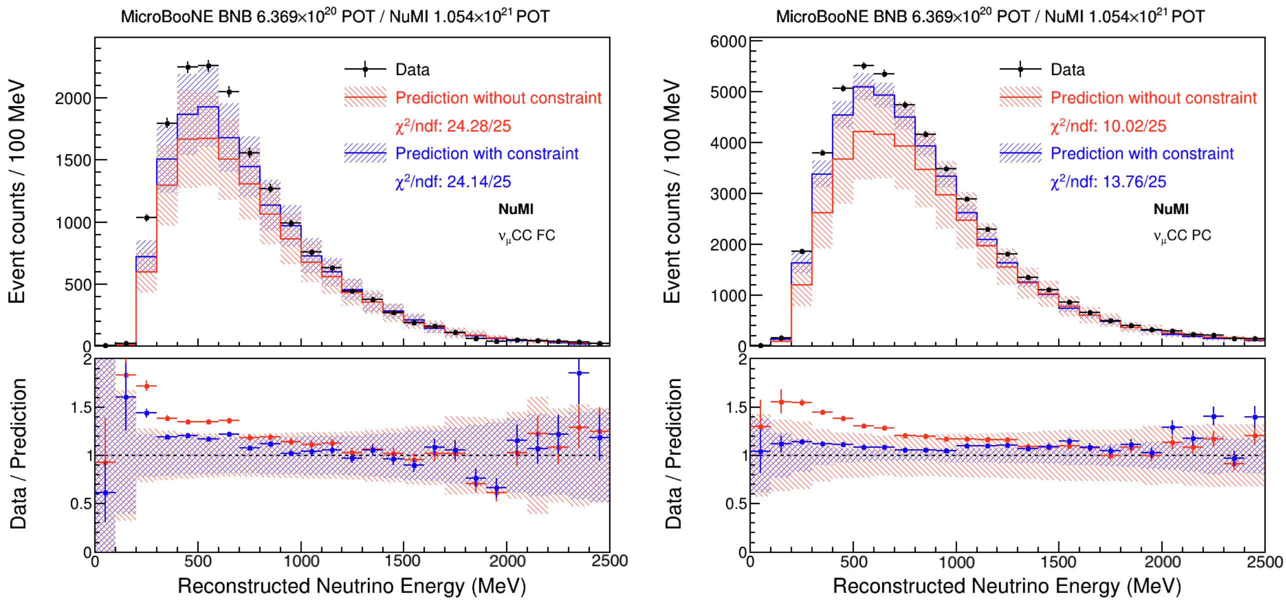

(a) NuMI Run1-3 ν_μ CC FC sample constrained by BNB Run1-3 ν_μ CC FC.

(b) NuMI Run1-3 ν_μ CC PC sample constrained by NuMI Run1-3 FC sample

Figure 6: (a) Reconstructed energy spectrum of NuMI Run1-3 ν_μ CC FC sample, constrained by BNB Run1-3 ν_μ CC FC. (b) Reconstructed energy spectrum of NuMI Run1-3 ν_μ CC PC sample, constrained by NuMI Run1-3 FC sample. The red (blue) histogram and band is MC prediction and its uncertainty before (after) the BNB ν_μ CC constraint. The bottom sub-panel presents the data-to-prediction ratio as well as the full systematic uncertainty of MC prediction.

3.2 Sensitivity Results

We have performed a sensitivity study in ν_e appearance and ν_e disappearance channels, using both the BNB and NuMI datasets. The sensitivity shown here is median sensitivity calculated using the frequenstist CLs method [29].

Figure 7 shows the ν_e appearance channel, with the full 3+1 oscillation sensitivity after profiling over the mixing angle $\sin^2\theta_{24}$, using the frequentist CLs method with 2000 pseudo experiments. Compared to the BNB-only result, the BNB and NuMI combined result improves the sensitivity significantly, as a result of breaking the degeneracy of oscillation parameters. With BNB and NuMI combined, the sensitivity covers the majority of the LSND 90% allowed region.

Figure 8 shows the ν_e disappearance channel. Similar to the ν_e appearance channel, the method of frequentist CLs was used to calculate profiled sensitivity for BNB-only and BNB/NuMI combined scenarios. By combining the BNB and NuMI, we recover the loss of sensitivity attributed to the parameter degeneracy and obtain s sensitivity that covers much of the Gallium result.

4 Summary

In this note, we present the 3+1 sterile neutrino oscillation analysis sensitivities using both the BNB and NuMI beams, built upon the previous result of BNB-only 3+1 oscillation analysis [25]. With flux model updates in MicroBooNE's simulation of the NuMI flux, we report the sensitivity results

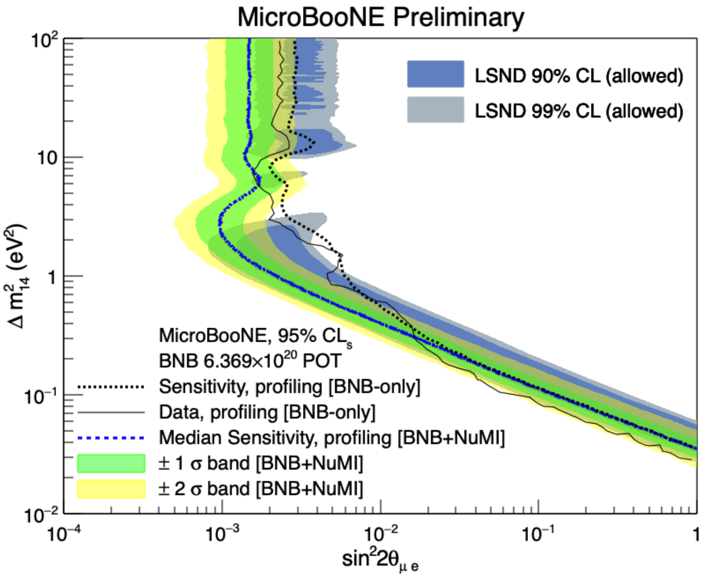

Figure 7: MicroBooNE 95% confidence level frequentist CLs limits in the Δm^2_{41} vs. $\sin^2 2\theta_{\mu e}$ parameter space. The LSND 90% and 95% CL allowed regions [14] are shown in shaded areas. The black dashed and solid lines are BNB-only sensitivity and data exclusion result, respectively, from previous result [25]. The blue dashed curve represents the MicroBooNE 95% CLs median sensitivity (2D profiling by minimizing over $\sin^2\theta_{24}$) in the full 3+1 oscillation scenario (both ν_e appearance and ν_e &ν_μ disappearance) using BNB Run1-3 and NuMI Run1-3 combined. The 1σ and 2σ bands around the median as shown as green and yellow shaded areas respectively.

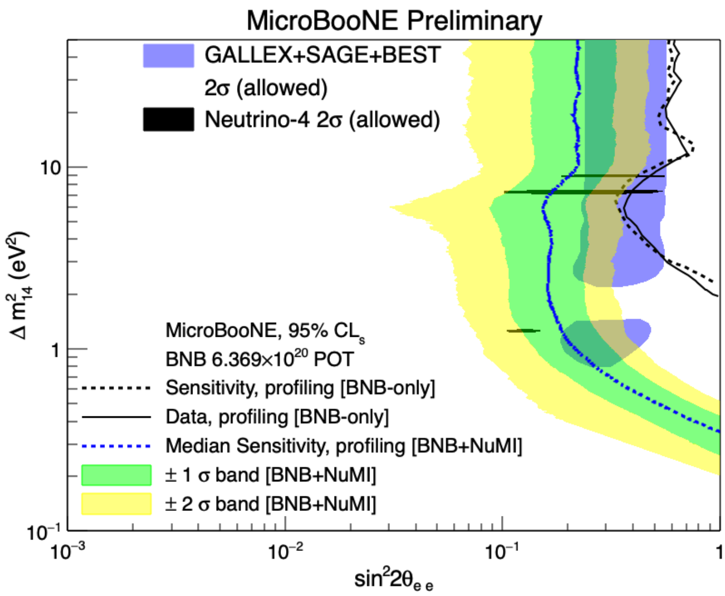

Figure 8: MicroBooNE 95% confidence level frequentist CLs limits in the Δm^2_{41} vs. $\sin^2 2\theta_{ee}$ parameter space. The GALLEX+SAGE+BEST [4] and Neutrino-4 [13] 2σ allowed regions are shown in shaded areas. The black dashed and solid lines are BNB-only sensitivity and data exclusion result, respectively, from previous result [25]. The blue dashed curve represents the MicroBooNE 95% CLs median sensitivity (2D profiling by minimizing over $\sin^2\theta_{24}$) in the full 3+1 oscillation scenario (both ν_e appearance and ν_e &ν_μ disappearance) using BNB Run1-3 and NuMI Run1-3 combined. The 1σ and 2σ bands around the median as shown as green and yellow shaded areas respectively.

for the full oscillation case that considers both the ν_e appearance and disappearance. The results show that adding the NuMI data to the analysis gains significant improvements in both channels, becoming sensitive to LSND and Gallium allowed regions. These gains follow from the different ν_μ -to-ν_e ratios in the NuMI and BNB beams, which significantly reduce the oscillation parameter degeneracy.

References

[1] P. Adamson et al. Improved Constraints on Sterile Neutrino Mixing from Disappearance Searches in the MINOS, MINOS+, Daya Bay, and Bugey-3 Experiments. *Phys. Rev. Lett.*, 125(7):071801, 2020.

[2] M. Andriamirado et al. Improved short-baseline neutrino oscillation search and energy spectrum measurement with the PROSPECT experiment at HFIR. *Phys. Rev. D*, 103(3):032001, 2021.

[3] F. Kaether, W. Hampel, G. Heusser, J. Kiko, and T. Kirsten. Reanalysis of the GALLEX solar neutrino flux and source experiments. *Phys. Lett. B*, 685:47–54, 2010.

[4] V. V. Barinov et al. Results from the Baksan Experiment on Sterile Transitions (BEST). 9 2021.

[5] J. N. Abdurashitov et al. Measurement of the solar neutrino capture rate with gallium metal. III: Results for the 2002–2007 data-taking period. *Phys. Rev. C*, 80:015807, 2009.

[6] G. Mention, M. Fechner, Th. Lasserre, Th. A. Mueller, D. Lhuillier, M. Cribier, and A. Letourneau. The Reactor Antineutrino Anomaly. *Phys. Rev. D*, 83:073006, 2011.

[7] Patrick Huber. On the determination of anti-neutrino spectra from nuclear reactors. *Phys. Rev. C*, 84:024617, 2011. [Erratum: Phys.Rev.C 85, 029901 (2012)].

[8] Th. A. Mueller et al. Improved Predictions of Reactor Antineutrino Spectra. *Phys. Rev. C*, 83:054615, 2011.

[9] F. P. An et al. Evolution of the Reactor Antineutrino Flux and Spectrum at Daya Bay. *Phys. Rev. Lett.*, 118(25):251801, 2017.

[10] F. P. An et al. Antineutrino energy spectrum unfolding based on the Daya Bay measurement and its applications. *Chin. Phys. C*, 45(7):073001, 2021.

[11] M. Estienne et al. Updated Summation Model: An Improved Agreement with the Daya Bay Antineutrino Fluxes. *Phys. Rev. Lett.*, 123(2):022502, 2019.

[12] C. Giunti, Y. F. Li, C. A. Ternes, and Z. Xin. Reactor antineutrino anomaly in light of recent flux model refinements, 10 2021.

[13] A. P. Serebrov et al. Search for sterile neutrinos with the Neutrino-4 experiment and measurement results. *Phys. Rev. D*, 104(3):032003, 2021.

[14] A. Aguilar-Arevalo et al. Evidence for neutrino oscillations from the observation of $\bar{\nu}_e$ appearance in a $\bar{\nu}_\mu$ beam. *Phys. Rev. D*, 64:112007, 2001.

[15] A. A. Aguilar-Arevalo et al. Improved Search for $\bar{\nu}_\mu \to \bar{\nu}_e$ Oscillations in the MiniBooNE Experiment. *Phys. Rev. Lett.*, 110:161801, 2013.

[16] A. A. Aguilar-Arevalo et al. Updated MiniBooNE neutrino oscillation results with increased data and new background studies. *Phys. Rev. D*, 103(5):052002, 2021.

[17] Carlo Giunti and T. Lasserre. eV-scale Sterile Neutrinos. *Ann. Rev. Nucl. Part. Sci.*, 69:163–190, 2019.

[18] Alexey Boyarsky, Oleg Ruchayskiy, and Mikhail Shaposhnikov. The role of sterile neutrinos in cosmology and astrophysics. *Annual Review of Nuclear and Particle Science*, 59(Volume 59, 2009):191–214, 2009.

[19] Laurent Canetti, Marco Drewes, Tibor Frossard, and Mikhail Shaposhnikov. Dark matter, baryogenesis and neutrino oscillations from right-handed neutrinos. *Phys. Rev. D*, 87:093006, May 2013.

[20] P. Abratenko et al. Search for an Excess of Electron Neutrino Interactions in MicroBooNE Using Multiple Final-State Topologies. *Phys. Rev. Lett.*, 128(24):241801, 2022.

[21] P. Abratenko et al. Search for an anomalous excess of charged-current quasielastic ν_e interactions with the MicroBooNE experiment using Deep-Learning-based reconstruction. *Phys. Rev. D*, 105(11):112003, 2022.

[22] P. Abratenko et al. Search for an anomalous excess of charged-current ν_e interactions without pions in the final state with the MicroBooNE experiment. *Phys. Rev. D*, 105(11):112004, 2022.

[23] P. Abratenko et al. Search for an anomalous excess of inclusive charged-current ν_e interactions in the MicroBooNE experiment using Wire-Cell reconstruction. *Phys. Rev. D*, 105(11):112005, 2022.

[24] A. A. Aguilar-Arevalo et al. Neutrino flux prediction at miniboone. *Phys. Rev. D*, 79:072002, Apr 2009.

[25] P. Abratenko et al. First constraints on light sterile neutrino oscillations from combined appearance and disappearance searches with the microboone detector. *Phys. Rev. Lett.*, 130:011801, Jan 2023.

[26] MicroBooNE doc-db 42272, "Updates to the NuMI Flux Simulation", The MicroBooNE Collaboration, https://microboone-docdb.fnal.gov/cgi-bin/sso/ShowDocument?docid=42272.

[27] Baobiao Yue, Wei Li, Jiajie Ling, and Fanrong Xu. A compact analytical approximation for a light sterile neutrino oscillation in matter. *Chin. Phys. C*, 44(10):103001, 2020.

[28] M.L. Eaton. Multivariate Statistics: A Vector Space Approach, 1983. John Wiley Sons, New York.

[29] A L Read. Presentation of search results: the cls technique. *Journal of Physics G: Nuclear and Particle Physics*, 28(10):2693, sep 2002.